Liquid-Crystalline Materials Based on Rhodium Carboxylate Coordination Polymers: Synthesis, Characterization and Mesomorphic Properties of Tetra(alkoxybenzoato)dirhodium(II) Complexes and Their Pyrazine Adducts

Marcia Rusjan,[†] Bertrand Donnio,[‡] Daniel Guillon,[‡] and Fabio D. Cukiernik*[,†,§]

INQUIMAE, Departamento de Química Inorgánica, Analítica y Química Física, Facultad de Ciencias Exactas y Naturales, Universidad de Buenos Aires, Pabellón II, Ciudad Universitaria, Núñez (C1428 EHA) Capital Federal, Argentina, Institut de Physique et Chimie des Matériaux de Strasbourg, UMR 7504 (CNRS-ULP), Groupe des Matériaux Organiques, 23 rue du Loess, 67037 Strasbourg Cedex, France, and Instituto de Ciencias, Universidad Nacional de General Sarmiento, Roca 850, San Miguel (1663), Provincia de Buenos Aires, Argentina

Received July 20, 2001. Revised Manuscript Received February 12, 2002

Tetra(alkoxybenzoato)dirhodium(II) complexes of the formula $Rh_2(x,y,z\text{-B}m\text{OC}n)_4$ (where B is the benzoate group; *m* is the number of alkoxy chains on the aromatic ring; *x*, *y*, and *z* are their positions of anchoring; and *n* is the number of carbon atoms in each alkoxy chain) and the corresponding pyrazine adducts have been synthesized and characterized. The pyrazine adducts were prepared to have a polymeric structure via connected metallic centers. The complexes synthesized are $Rh_2(3,4,5\text{-B3OC}n)_4$ for $n = 8$, 10, 14, and 18; $Rh_2(3,4\text{-B2OC}n)_4$ for $n = 9$, 14, and 18; and $Rh_2(3,5\text{-B2OC}n)_4$ for $n = 9$ and 18, as well as the corresponding pyrazine adducts $[Rh_2(3,4,5\text{-B3OC}n)_4pz]_x$ for $n = 10$, 14, and 18; $[Rh_2(3,4\text{-B2OC}n)_4pz]_x$ for $n = 14$ and 18; and $[Rh_2(3,5\text{-B2OC}n)_4pz]_x$ for $n = 9$ and 18. Their liquid-crystalline (LC) properties have been analyzed. Most of them exhibit LC columnar and cubic mesophases with melting transition temperatures close to or even below room temperature. The mesomorphic character of the pyrazinic compounds, compared to the nonmesomorphic aliphatic carboxylate analogues, can be interpreted in terms of the ability of the equatorial ligands to fill the interdimeric space efficiently. Some internal characteristics about the arrangement of the molecules inside the columns are discussed.

Introduction

Liquid-crystalline coordination polymers form a class of materials expected to present the properties of both coordination polymers (complexes in which the metallic centers are bridged by appropriate ligands, giving extended structures)[1−3] and metallomesogens (metal-containing liquid crystals).[4−8] The interest in such compounds arises mainly from the possibility of combining the properties of 1-D or 2-D organized metallic centers, such as high electric conductivity,[2,9] ferrimagnetic behavior,[10,11] ferroelectricity,[1,12] or 1-D energy transport,[13] with the fluidity and anisotropy of liquid-crystalline phases and the processability of polymers.

Polymeric metallomesogens[14] can be classified according to the position of the metallic atoms as main-chain, side-chain, or cross-linked. Several examples exhibiting nematic and smectic mesophases are known in each of

* Correspondence e-mail: fabioc@qi.fcen.uba.ar.
[†] Universidad de Buenos Aires.
[‡] Groupe des Matériaux Organiques.
[§] Universidad Nacional de General Sarmiento.

(1) Chen, C. T.; Susslick, K. S. *Coord. Chem. Rev.* **1993**, *28*, 293.
(2) Kellogg, G. E.; Gaudiello, J. G. In *Inorganic Materials*; Bruce, D. W., O'Hare, D., Eds.; John Wiley & Sons: New York, 1992; p 353.
(3) Robson, R. *J. Chem. Soc., Dalton Trans.* **2000**, 3735.
(4) Serrano, J. L., Ed. *Metallomesogens*; VCH: Weinheim, Germany, 1996.
(5) (a) Giroud-Godquin, A. M. In *The Handbook of Liquid Crystals*; Goodby, J. W., Ed.; VCH: Weinheim, Germany, 1997. (b) Giroud-Godquin, A. M.; Maitlis, P. M. *Angew. Chem., Int. Ed. Engl.* **1991**, *30*, 375.
(6) Donnio, B.; Bruce, D. W. *Struct. Bonding (Berlin)* **1999**, *95*, 193.
(7) Espinet, P.; Esteruelas; M. A.; Oro, L. A.; Serrano, J. L.; Solá, E. *Coord. Chem. Rev.* **1992**, *117*, 215.
(8) Bruce, D. W. In *Inorganic Materials*; Bruce, D. W., O'Hare, D., Eds.; John Wiley & Sons: New York, 1992; p 405.
(9) Schultz, H.; Lehmann, H.; Rein, M.; Hannack, M. *Struct. Bonding (Berlin)* **1991**, *74*, 41.
(10) Caneschi, A.; Gatteschi, D.; Sessoli, R.; Rey, P. *Acc. Chem. Res.* **1989**, *22*, 392.
(11) Kahn, O. *Molecular Magnetism*; VCH: Weinheim, Germany, 1992.
(12) Susslick, K. S.; Chen, C. T. *Polym. Mater. Sci. Eng.* **1990**, *63*, 272.
(13) (a) *Phthalocyanines. Properties and Applications*; Leznoff, C. C., Lever, A. B. P., Eds.; VCH: New York, 1993. (b) Simmon, J.; Bassoul, J. M. In *Phthalocyanines. Properties and Applications*; Leznoff, C. C., Lever, A. B. P., Eds.; VCH: New York, 1993; p 287.
(14) (a) Oriol, L. In *Metallomesogens*; Serrano, J. L., Ed.; VCH: Weinheim, Germany, 1996; pp 193−231. (b) Oriol, L.; Serrano, J. L. *Adv. Mater.* **1995**, *7*, 348. (c) Oriol, L.; Piñol, M.; Serrano, J. L. *Prog. Polym. Sci.* **1997**, *22*, 873.

10.1021/cm0109995 CCC: $22.00
Published on Web 03/22/2002

these categories; however, there are few examples of systems showing columnar structures.[14−16] With very few exceptions, metallomesogens all belong to the main-chain type and fall into two main groups. In the first group ("strong polymers"), the metal atoms are axially bridged by neutral or anionic ligands, as in some phthalocyanine[13] derivatives and mixed-valent diruthenium carboxylates.[17−19] In the second group (sometimes referred to as "pseudo-polymeric systems"), the metal atoms are bound by weaker intermolecular coordination between "discrete" molecular units, as in some vanadyl β-diketonates[20] or some bimetallic carboxylates.[21−23] In the last case, the intermolecular links found in the crystalline phase for the unsolvated copper[24] and rhodium[25] alkanoates—where the axial positions are occupied by oxygen atoms of neighboring molecules—are preserved in the LC phase, giving rise to a 2-D hexagonal arrangement of columns.

These electron-rich bimetallic carboxylates with a "lantern structure" are powerful building blocks for 1-D coordination polymers, and interesting examples of both main-chain and side-chain polymers have been reported in the literature.[22c,26] Long-chain divalent copper, rhodium, ruthenium, molybdenum, and chromium carboxylates (without axial ligands) present thermotropic columnar mesophases.[21−23] These facts prompted their use in the search of LC polymeric systems.

A suitable ligand often used to "connect" metallic centers is pyrazine (pz), and indeed, many efforts have been directed toward the synthesis of such $[M_2(O_2CR)_4pz]_\infty$ 1-D polymers. Unfortunately, all of the compounds obtained so far, namely, $Cu_2(O_2CC_{n-1}H_{2n-1})_4pz$ ($n = 10, 16$),[22b] $Ru_2(O_2CC_{11}H_{23})_4pz$,[22f] and Rh_2(4-B1OC8)$_4$pz,[27] have not revealed any mesomorphic behavior. The copper derivatives polymerized by 4,4'-bipyridine did not produce mesophases either.[22b] The only compound that appeared promising was a copper branched-chain carboxylate, although a detailed characterization of its mesophase was not obtained.[22b] The absence of mesomorphism in these compounds was explained on the basis of space-filling requirements.[22f,28] The intercalation of pyrazine between the binuclear units creates a void space that needs to be filled to obtain a stable condensed phase; when the carboxylates bear only one chain, the interdimeric space is likely to be filled by the aliphatic chains belonging to a adjacent polymeric strand, giving rise to a crossed-supramolecular structure that prevents the formation of a columnar mesophase (which needs a parallel arrangement of columns). A similar situation was found in mixed-valent diruthenium carboxylates (with small axial anions such as Cl^- playing the role of pyrazine). However, liquid-crystalline behavior was induced by using bulky equatorial ligands bearing two and three aliphatic chains; with such ligands, it was possible to fill correctly the interdimeric space and thus to induce a thermotropic columnar mesophase.[17,18]

Using the same strategy, we report herein the results obtained with pyrazine-polymerized divalent rhodium carboxylates. The synthesis, characterization, and mesomorphic properties of nonpolymeric dirhodium tetracarboxylates derived from 3,4-disubstituted, 3,5-disubstituted, and 3,4,5-trisubstituted alkoxybenzoates [denoted, respectively, Rh_2(3,4-B2OCn)$_4$, Rh_2(3,5-B2OCn)$_4$, and Rh_2(3,4,5-B3OCn)$_4$ and depicted in Scheme 1], as well as their polymeric pyrazine adducts, are described. This study is an extension of the work by Serrano et al.[27] on mesogenic rhodium benzoates: they studied a series of dirhodium Rh_2(4-B1OCn)$_4$ (n = 8−14) complexes and the pyrazine adduct of the octyl derivative, $[Rh_2$(4-B1OCn)$_4$pz$]_n$, as well as the Rh_2(3,4-B2OC10)$_4$ and Rh_2(3,4,5-B3OC10)$_4$ compounds. The present study is focused on bi- and trisubstituted alkoxy benzoates with the aim, on one hand, to induce mesomorphism to the pyrazine-polymerized systems and, on the other hand, to correlate the aliphatic-chain substitution pattern on the aromatic ring with these mesomorphic properties.

Experimental Section

Synthesis. The syntheses of the alkoxybenzoic acids used as ligands were carried out following published procedures[17,29] and purified by chromatography on silica gel. They all gave satisfactory ^{1}H NMR and IR spectra, as well as elemental analyses.

(15) Valdebenito, N.; Oriol, L.; Barberá, J.; Diaz, F.; Serrano J. L. *Macromol. Chem. Phys.* **2000**, *201*, 2573.
(16) Guillon, D. *Struct. Bonding (Berlin)* **1999**, *95*, 42.
(17) Cukiernik, F. D.; Ibn-Elhaj, M.; Chaia, Z.; Marchon, J. C.; Giroud-Godquin, A. M.; Guillon, D.; Skoulios, A.; Maldivi, P. *Chem. Mater.* **1998**, *10*, 83.
(18) Chaia, Z.; Heinrich, B.; Cukiernik, F. D.; Guillon, D. *Mol. Cryst. Liq. Cryst.* **1999**, *330*, 213.
(19) Caplan, J. F.; Murphy, C. A.; Swansburg, S.; Lemieux, R. P.; Cameron, T. S.; Aquino, M. A. S. *Can. J. Chem.* **1998**, *76*, 1520.
(20) Kilian, D.; Knawby, D.; Athanassopoulou, M. A.; Trzaska, S. T.; Swager, T. M.; Wrobel, S.; Haase, W. *Liq. Cryst.* **2000**, *27*, 209.
(21) Marchon, J. C.; Maldivi, P.; Giroud-Godquin, A. M.; Guillon, D.; Ibn-Elhaj, M.; Skoulios, A. In *Nanostructures Based on Molecular Materials*; Göpel, W., Ziegler, C., Eds.; VCH: Weinheim, Germany, 1992; p 285 and references therein.
(22) (a) Marchon, J. C.; Maldivi, P.; Giroud-Godquin, A. M.; Guillon, D.; Skoulios, A.; Strommen, D. P. *Philos. Trans. R. Soc. London* **1990**, *A330*, 109. (b) Attard, G. S.; Cullum, P. R. *Liq. Cryst.* **1990**, *8*, 299. (c) Attard, G. S.; Templer, R. H. *J. Mater. Chem.* **1993**, *3*, 207. (d) Maldivi, P.; Bonnet, L.; Giroud-Godquin, A. M.; Ibn-Elhaj, M.; Guillon, D.; Skoulios, A. *Adv. Mater.* **1993**, *5*, 909. (e) Terech, P.; Schaffhauser, V.; Maldivi, P.; Guenet, J. M. *Europhys. Lett.* **1992**, *17*, 515. (f) Bonnet, L.; Cukiernik, F. D.; Maldivi, P.; Giroud-Godquin, A. M.; Marchon, J. C.; Ibn-Elhaj, M.; Guillon, D.; Skoulios, A. *Chem. Mater.* **1994**, *6*, 31. (g) Baxter, D. V.; Cayton, R. H.; Chisholm, M. H.; Huffman, J. C.; Putilina, E. F.; Tagg, S. L.; Wesemann, J. L.; Zwanziger, J. W.; Darrington, F. D. *J. Am. Chem. Soc.* **1994**, *116*, 4551. (h) Cayton, R. H.; Chisholm, M. H.; Huffmann, J. C.; Lobkovsky, E. B. *J. Am. Chem. Soc.* **1991**, *113*, 8709.
(23) (a) Abied, H.; Guillon, D.; Skoulios, A.; Dexter, H.; Giroud-Godquin, A. M.; Marchon, J. C. *J. Phys. Fr.* **1988**, *49*, 345. (b) Maldivi, P.; Guillon, D.; Giroud-Godquin, A. M.; Marchon, J. C.; Abied, H.; Dexter, H.; Skoulios, A. *J. Chim. Phys.* **1989**, *86*, 1651. (c) Ibn-Elhaj, M.; Guillon, D.; Skoulios, A.; Maldivi, P.; Giroud-Godquin, A. M.; Marchon, J. C. *J. Phys. II* **1992**, *2*, 2237. (d) Poizat, O.; Strommen, D.; Maldivi, P.; Giroud-Godquin, A. M.; Marchon, J. C. *Inorg. Chem.* **1990**, *29*, 4853. (e) Bardet, M.; Maldivi, P.; Giroud-Godquin, A. M.; Marchon, J. C. *Langmuir* **1995**, *11*, 2306.
(24) (a) Lomer, T. R.; Perera, K. *Acta Crystallogr.* **1974**, *B30*, 2912. (b) Lomer, T. R.; Perera, K. *Acta Crystallogr.* **1974**, *B30*, 2913. (c) Campbell, G. C.; Haw, J. F. *Inorg. Chem.* **1988**, *27*, 3706.
(25) Cotton, F. A.; Shiu, K. B. *Rev. Chim. Miner.* **1986**, *23*, 14.
(26) (a) Valentine, J. S.; Silverstein, A. J.; Soos, Z. G. *J. Am. Chem. Soc.* **1974**, *96*, 97. (b) Cukiernik, F. D.; Giroud-Godquin, A. M.; Maldivi, P.; Marchon, J. C. *Inorg. Chim. Acta* **1994**, *215*, 203. (c) Beck, E. J.; Drysdale, K. D.; Thompson, L. K.; Li, L.; Murphy, C. A.; Aquino, M. A. S. *Inorg. Chim. Acta* **1998**, *279*, 121. (d) Mikuriya, M.; Nukada, R.; Morishita, H.; Handa, M. *Chem. Lett.* **1995**, 617 (e) Cotton, F. A.; Kim, Y. *J. Am. Chem. Soc.* **1993**, *115*, 8511 (f) Cotton, F. A.; Kim, Y.; Lu, J. *Inorg. Chim. Acta* **1994**, *221*, 1.
(27) Barberá, J.; Esteruelas, M. A.; Levelut, A. M.; Oro, L. A.; Serrano, J. L.; Solá, E. *Inorg. Chem.* **1992**, *31*, 732.
(28) Cukiernik, F. D. Ph.D. Thesis, University of Grenoble, 1993.
(29) Strzelecka, H.; Jallabert, C.; Veber, M.; Malthête, J. *Mol. Cryst. Liq. Cryst.* **1988**, *156*, 347.

Scheme 1

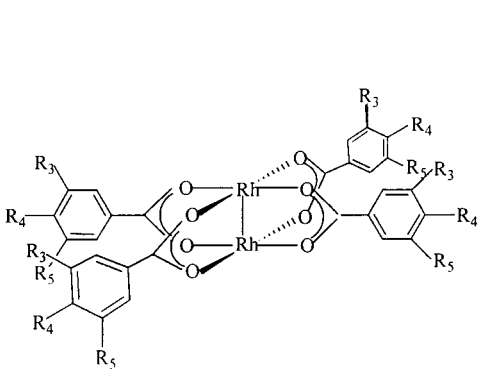

1a-9a

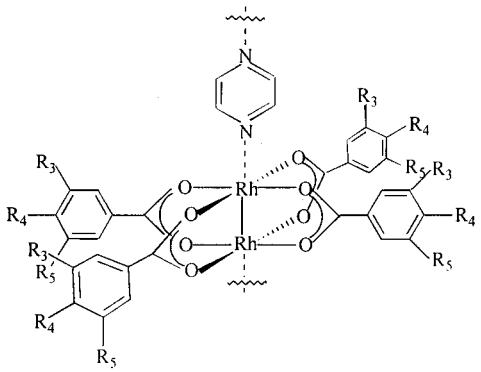

1b-9b

R_3	R_4	R_5	without pyrazine		with axial pyrazine	
$OC_{18}H_{37}$	$OC_{18}H_{37}$	$OC_{18}H_{37}$	**1a**	Rh_2(3,4,5-B3OC18)$_4$	**1b**	Rh_2(3,4,5-B3OC18)$_4$pz
$OC_{14}H_{29}$	$OC_{14}H_{29}$	$OC_{14}H_{29}$	**2a**	Rh_2(3,4,5-B3OC14)$_4$	**2b**	Rh_2(3,4,5-B3OC14)$_4$pz
$OC_{10}H_{21}$	$OC_{10}H_{21}$	$OC_{10}H_{21}$	**3a**	Rh_2(3,4,5-B3OC10)$_4$	**3b**	Rh_2(3,4,5-B3OC10)$_4$pz
OC_8H_{17}	OC_8H_{17}	OC_8H_{17}	**4a**	Rh_2(3,4,5-B3OC8)$_4$		-
$OC_{18}H_{37}$	$OC_{18}H_{37}$	H	**5a**	Rh_2(3,4-B2OC18)$_4$	**5b**	Rh_2(3,4-B2OC18)$_4$pz
$OC_{14}H_{29}$	$OC_{14}H_{29}$	H	**6a**	Rh_2(3,4-B2OC14)$_4$	**6b**	Rh_2(3,4-B2OC14)$_4$pz
OC_9H_{19}	OC_9H_{19}	H	**7a**	Rh_2(3,4-B2OC9)$_4$		-
$OC_{18}H_{37}$	H	$OC_{18}H_{37}$	**8a**	Rh_2(3,5-B2OC18)$_4$	**8b**	Rh_2(3,5-B2OC18)$_4$pz
OC_9H_{19}	H	OC_9H_{19}	**9a**	Rh_2(3,5-B2OC9)$_4$	**9b**	Rh_2(3,5-B2OC9)$_4$pz

Nonpolymeric Compounds: Rh_2(3,4,5-B3OC*n*)$_4$ for *n* = 18 (1a), 14 (2a), 10 (3a), and 8 (4a); Rh_2(3,4-B2OC*n*)$_4$ for *n* = 18 (5a), 14 (6a), and 9 (7a); and Rh_2(3,5-B2OC*n*)$_4$ for *n* = 18 (8a) and 9 (9a). The products were synthesized by a modification of the methods already published,[27] i.e., by metathesis of the acetate ligand from the commercially available $Rh_2(\mu\text{-}O_2CCH_3)_4$ in a 3−4-fold excess of the ligands (melt, no added solvent) magnetically stirred for 6 h under N_2(g) atmosphere. The products thus obtained were treated with hot heptane and filtered to eliminate the excess of rhodium acetate. Then, they were cooled until the excess of alkoxybenzoic ligand precipitated and filtered again (except for compound **4a**, for which the ligand was soluble even at very low temperature). The green solutions were concentrated under reduced pressure to about 3 mL, and ethanol (for **1a**, **2a**, **4a**, **8a**, and **9a**) or acetone (for **3a** and **5a**−**7a**) was added until the blue solvent adducts precipitated, at which time they were filtered under reduced pressure. The solids were dissolved in $CHCl_3$, 3−4 mL of ethanol (for **1a**, **2a**, and **5a**) or methanol (for **3a**, **4a**, and **6a**−**9a**) was added, and the mixtures were heated until complete dissolution. After the evaporation of $CHCl_3$, the products precipitated, and the solutions were decanted to eliminate the excess of ligand (this procedure was repeated several times until complete elimination of the free ligand). The solids were dried at 80 °C for 60 h in a vacuum oven to give the green products.

Polymeric Pyrazine Adducts: [Rh_2(3,4,5-B3OC*n*)$_4$pz]$_x$ for *n* = 18 (1b), 14 (2b), and 10 (3b); [Rh_2(3,4-B2OC*n*)$_4$pz]$_x$ for *n* = 18 (5b) and 14 (6b); and [Rh_2(3,5-B2OC*n*)$_4$pz]$_x$ for *n* = 18 (8b) and 9 (9b). The corresponding rhodium compounds were dissolved in $CHCl_3$, and a 2-fold excess of pyrazine (in the same solvent) was added dropwise with magnetic stirring. The green solutions became dark red, and after being stirred for another 30 min, they were evaporated to dryness under a vacuum. Ten milliliters of ethanol was added twice to the solids, and the suspensions were sonicated and filtered to eliminate the excess of pyrazine. The compounds were dried under a vacuum for 24 h. Attempts to synthesize adducts failed for some of the compounds: binding the pyrazine in stoichiometric amounts appeared impossible (a deficiency of the ligand was observed). No excess of pyrazine (di-adduct) was observed under the conditions of the synthesis.

Characterization. The characterization of the synthesized compounds was carried out by IR spectroscopy using KBr pellets of the samples on a Nicolet FTIR 510P spectrometer, by elemental analyses either at INQUIMAE (Carlo Erba CHNS-O EA1108) or at the Service d'Analyse de l'Institut Charles Sadron (Strasbourg, France), and by ^{1}H NMR spectroscopy of the samples in $CDCl_3$ on a Bruker AC200 spectrometer. Solution electronic spectra (see below) were recorded with a Hewlett-Packard 8453 instrument. The obtained microanalytical data and yields are presented in Table 1 for each compound. IR and ^{1}H NMR spectra were identical (excluding the expected differences in the IR band intensities and NMR peak integrations) for all of the members of each series of compounds and were used as additional evidence; their main features are analyzed under the Results section.

Physicochemical Measurements. Optical microscopy observations as a function of temperature were carried out on a Leitz DMRX microscope equipped with a Leitz 1350 hot-stage device. The compounds were observed between cross polarizers at a heating rate of 5 °C/min. The pyrazine adducts were heated only to 110−130 °C to avoid decomposition (see below). Transition temperatures and enthalpies were obtained by DSC experiments at a heating rate of 5 °C/min on a Shimadzu DSC-50 instrument equipped with a low-temperature LTC-50 device using 2.0 ± 0.2 mg samples in all cases. The onset temperatures were used as transition temperatures. XRD patterns were obtained with two different experimental setups, the crude powder being filled in Lindemann capillaries of 1 mm diameter. A linear monochromatic Cu Kα_1 beam (λ =

Table 1. Elemental Analyses and Yields[a] of the Synthesized Monomeric (1a−9a) and Polymeric (1b−9b) Compounds

	analysis found (calc)		yield		analysis found (calc)		
compd	C (%)	H (%)	(%)	compd	C (%)	H (%)	N (%)
1a	75.20 (74.92)	11.68 (11.65)	45	**1b**	74.42 (74.61)	11.62 (11.51)	0.76 (0.70)
2a	73.21 (72.70)	11.13 (11.08)	39	**2b**	72.40 (72.38)	10.99 (10.93)	0.84 (0.84)
3a	68.52 (69.29)	10.05 (10.22)	63	**3b**	68.81 (69.01)	10.17 (10.06)	0.86 (1.05)
4a	66.45 (66.82)	9.72 (9.60)	81				
5a	72.57 (72.79)	10.96 (10.94)	35	**5b**	72.08 (72.43)	10.68 (10.78)	1.19 (0.96)
6a	70.34 (70.38)	10.37 (10.29)	66	**6b**	69.78 (70.04)	10.05 (10.12)	1.41 (1.14)
7a	65.76 (65.70)	9.11 (9.04)	94				
8a	10.83 (10.93)	10.83 (10.93)	61	**8b**	72.46 (72.44)	10.89 (10.78)	0.95 (0.96)
9a	65.83 (65.70)	8.88 (9.04)	89	**9b**	65.93 (65.47)	8.87 (8.87)	1.46 (1.47)

[a] Yields of pirazine adducts were all higher than 80%.

1.5418 Å) was obtained using a Guinier camera (900 W) or a Debye−Scherrer camera, both equipped with a bent quartz monochromator and an electric oven. A first set of diffraction patterns was registered with an Inel CPS 120 gas curved counter associated with a data-acquisition computer system; periodicities up to 60 Å could be measured, and the sample temperature was controlled to within ±0.05 °C. The second set of diffraction patterns was registered on an image plate; the cell parameters were calculated from the positions of the reflections at the smallest Bragg angle, which, in all cases, were the most intense. Periodicities up to 90 Å could be measured, and the sample temperature was controlled to within ±0.3 °C. In each case, the exposure time was varied from 1 to 24 h. The XRD patterns were carried out between room temperature and 110−130 °C for the pyrazine adducts and between room temperature and 200 °C for the other compounds.

Results

Synthesis and Characterization of the Nonpolymeric Complexes. The $Rh_2(BmOCn)_4$ complexes **1a**−**9a** were prepared by exchange reactions of the equatorial ligands, which likely proceed via a mechanism that was already determined[30] for rhodium acetate. They are all soluble in $CHCl_3$, CH_2Cl_2, and heptane. When treated with methanol, ethanol, ether, or acetone, light blue adducts were formed. These bis-solvato adducts are generally insoluble in the respective solvents; the solubility increases when the aliphatic part is reduced either by short chains or by a reduced number of chains. The green color of the solid unsolvated species, as well as that seen in $CHCl_3$ solutions, is due to the two bands present in the visible region: band I at 664 nm and band II at 421 nm, assigned to π^* Rh−Rh → σ^* Rh−Rh and to π^* Rh−Rh → s* Rh−(Rh−O) transitions, respectively.[31]

Characterization of all of the $Rh_2(BmOCn)_4$ compounds was completed by ^{1}H NMR and IR spectroscopies. The ^{1}H NMR ($CDCl_3$) spectra of the various series included peaks at the following values of δ: for the Rh_2-(3,4,5-B3OC*n*)$_4$ series, 7.25 (s, 8H, H2/H6−C_6H_2−), 3.83 (m, 24H, −OCH_2−), 1.2−1.7 [m, 24(n − 2)H, other −CH_2− groups], 0.87 (t, 36H, −CH_3); for the Rh_2(3,4-B2OC*n*)$_4$ series, 7.61 (d, 4H, H6−C_6H_3−, J = 8.4 Hz), 7.53 (s, 4H, H2−C_6H_3−), 6.67 (d, 4H, H5−C_6H_3−, J = 8.4 Hz), 3.86 (dt, 16H, −OCH_2−, J = 6.2−6.6 Hz), 1.2−1.7 [m, 16(n − 2)H, other −CH_2− groups], 0.87 (m, 24H, −CH_3); and for the Rh_2(3,5-B2OC*n*)$_4$ series, 7.16 (d, 8H, H2/H6−C_6H_3−, J = 2 Hz), 6.45 (t, 4H, H4−C_6H_3−, J = 2 Hz), 3.79 (t, 16H, −OCH_2−), 1.2−1.7 [m, 16(n − 2)H, other −CH_2− groups], 0.87 (t, 24H, −CH_3).

The IR spectra of all of these compounds exhibited typical bands in the 1350−1600 cm^{-1} region: a sharp one at 1468 cm^{-1} with a shoulder at 1464 cm^{-1} (δCH_2-asym of CH_2 and CH_3, respectively), the corresponding δCH_3sym (CH_3) band at 1376 cm^{-1}, and the δCH_2asym (α to the ether group) band at 1420−1425 cm^{-1}, as well as the quadrant and semicircle aromatic ring vibration modes[32] at ca. 1560 cm^{-1} for the 3,4,5 series (overlapped with a carbonyl stretch at 1558 cm^{-1}; see below), at 1600 and 1517 cm^{-1} for the 3,4 series, and as a double peak at 1608 cm^{-1} for the 3,5 series. The CO_2 stretching modes were also detected (and assigned after careful comparisons among the whole series and assignments for the other vibrational modes)[32] at 1558 cm^{-1} (νCO_2-asym) and 1409 cm^{-1} (νCO_2sym) for the Rh_2(3,4,5-B3OC*n*)$_4$ series, at 1552 cm^{-1} (νCO_2asym) and 1384 cm^{-1} (νCO_2sym) for the Rh_2(3,4-B2OC*n*)$_4$ series, and at 1564 cm^{-1} (νCO_2asym) and 1408 cm^{-1} (νCO_2sym) for the Rh_2(3,5-B2OC*n*)$_4$ series. The Δ CO_2asym−sym gap was therefore calculated for each series as 149, 168, and 156 cm^{-1} respectively, suggesting that the asymmetry in the ring substitution is reflected in the coordination symmetry;[33] however, in the absence of structural data, no further conclusions can be drawn.

Solution Formation of Pyrazine Adducts. The green $CHCl_3$ solutions of complexes **1a**−**9a** became red upon the addition of pyrazine. A spectrophotometric titration of **1a** by pyrazine gave the results presented in Figure 1. For pz/$Rh_2(BmOCn)_4$ molar ratios (x) ranging from 0 to 0.5, band I originally at 664 nm shifted to 577 nm (isosbestic point at 625 nm), whereas band II located at 421 nm for the unligated dimer remained nearly constant, as expected.[31] In the present case, however, this band was superimposed on a new and strong band at ca. 424 nm, probably due to a Rh_2 → pz π^* MLCT.

For x = 0.5−1, the band at 425 nm transformed into a new one at 372 nm, probably with the same origin, with an isobestic point at 395 nm. The band at 577 nm remained unchanged. For x above 1, the band at 577 nm decreased, and a new band appeared at 530 nm, with an isosbestic point at 542 nm. These spectral changes show that a complex process involving four

(30) Bear, J. L.; Kitchens, J.; Wilcott III, M. R. *J. Inorg. Nucl. Chem.* **1971**, *33*, 3479.
(31) Boyar, E.; Robinson, S. *Coord. Chem. Rev.* **1983**, *50*, 109.
(32) Lin-Vien, D.; Colthup, N.; Fateley, W.; Grasselli, J. *The Handbook of Infrared and Raman Characteristic Frequencies of Organic Molecules*; Academic Press: New York, 1991.
(33) Deacon, G.; Phillips, R. *Coord. Chem. Rev.* **1980**, *33*, 227.

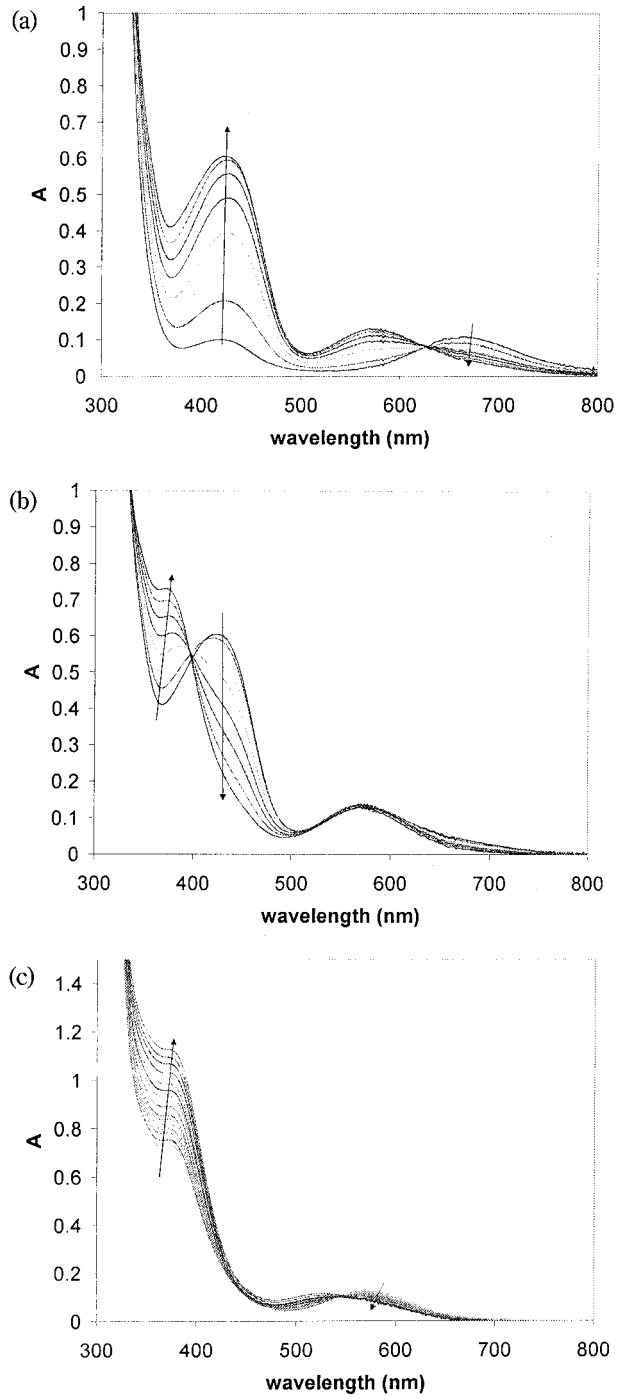

Figure 1. Solution absorbance as a function of wavelength for increasing molar fractions of pyrazine. Divided in three sequences according to the molar fraction of pirazine added: (a) from 0 to 0.5, (b) from 0.5 to 1, and (c) greater than 1. The arrows indicate the direction in which the molar fraction of pirazine increases.

different species was operative. The following mechanism agrees with the experimental observations:

$$\mathbf{1a} + \mathrm{pz} \leftrightarrow \mathbf{1a}\text{–}\mathrm{pz} \quad (1a)$$

$$\mathbf{1a}\text{–}\mathrm{pz} + \mathbf{1a} \leftrightarrow \mathbf{1a}\text{–}\mathrm{pz}\text{–}\mathbf{1a} \quad (1b)$$

$$\mathbf{1a}\text{–}\mathrm{pz}\text{–}\mathbf{1a} + \mathrm{pz} \leftrightarrow (\mathbf{1a}\text{–}\mathrm{pz})_n \quad (2)$$

$$(\mathbf{1a}\text{–}\mathrm{pz})_n + \mathrm{pz} \leftrightarrow \mathrm{pz}\text{–}\mathbf{1a}\text{–}\mathrm{pz} \quad (3)$$

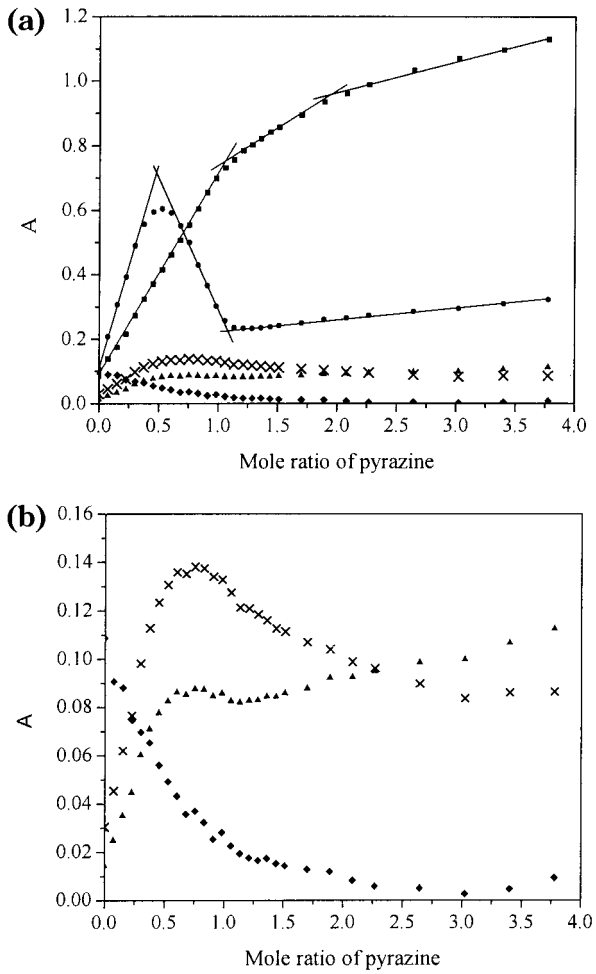

Figure 2. Solution absorbance as a function of the molar fraction of pyrazine for the maxima of the different peaks. (a) ◆, 664 nm; ▲, 530 nm; ×, 577 nm; ●, 425 nm; ■, 372 nm. The solid lines show the slope changes in the absorbance in the most strong bands. (b) Detail of 577, 664, and 530 nm. All of the spectra were corrected (considering a linear relationship between absorbance and concentration) to a concentration of 5.97×10^{-5} M, which is the initial concentration.

In fact, for $0 < x < 0.5$, the large excess of complex warrants the formation of **1a**–pz–**1a** as the dominant species; consequently, eqs 1a and 1b can be unified in

$$2(\mathbf{1a}) + \mathrm{pz} \leftrightarrow \mathbf{1a}\text{–}\mathrm{pz}\text{–}\mathbf{1a} \quad (1)$$

The spectral results suggest that these three processes are quite well separated; then, there is a clear predominant species in each x domain.

These considerations are supported by the mole ratio plot[34] shown in Figure 2. The band at 425 nm has a pronounced maximum at $x = 0.5$, in agreement with the slope change in the 577-nm absorbance trace, thus confirming the **1a**–pz–**1a** formulation for the species forming at this stage. The band at 372 nm has a marked change in slope up to $x = 1$ and a second one near $x = 2$, corresponding to the 1:1 polymeric species and the pz–**1a**–pz bis-adduct, respectively. The band at 667 nm also decreases to almost zero at $x = 1$. Similar results have been obtained with diruthenium aliphatic carbox-

(34) Reilley, C. N.; Sawyer, D. T. *Experiments for Instrumental Methods*; McGraw-Hill: New York, 1961.

ylates.[35] In the present case, the formulation of the 1:1 species as polymeric is based not only on coordination chemistry considerations, but also on experimental spectroscopic evidence (see below). A value on the order of 10^9 was estimated from the data on Figure 2 for the equilibrium constant K_1.

Synthesis and Characterization of the Polymeric Pyrazine Adducts. The UV−vis spectral results just discussed suggest that compounds of different stoichiometries could be obtained from solutions containing mixtures of $Rh_2(BmOCn)_4$ and pyrazine. An equimolar mixture seems to be the best way to produce a 1:1 polymer as the main species in solution. However, evaporation—and subsequent purification—of the solutions obtained under the conditions described in the Experimental Section (excess of pyrazine in the original solution) gave the 1:1 polymeric adducts **1b**−**9b**, as revealed by different techniques. The pyrazine/Rh_2-($BmOCn$)$_4$ ratios of the final solids obtained from different solution mixtures were monitored by the ratio between the ^{1}H NMR peaks due to pyrazine hydrogen atoms and those due to aromatic carboxylate hydrogen atoms: a 2-fold excess of pyrazine in solution appeared to be necessary to obtain a 1:1 stoichiometry in the final solid adducts. Elemental analysis results were in agreement with the 1:1 stoichiometry, and even stronger evidence came from spectroscopic probes.

Indeed, the IR spectra of the obtained compounds were almost identical to those obtained for $Rh_2(BmOCn)_4$ species, except for a slight shift (3−5 cm^{-1}) to higher energy in the νCO_2asym stretching. No significant extra peaks were observed; in particular, the absence of any signal due to monocoordinated pyrazine ruled out the possible existence of species containing nonbridged pyrazine.

The ^{1}H NMR spectra of the polymeric adducts were consistent with the proposed structure. The ratios between the integrated aromatic resonances of the benzoates and those of the pyrazines were equal to 8/4 for **1b**−**3b** and 12/4 for **5b**, **6b**, **8b**, and **9b**, as expected. The spectra of the $[Rh_2(3,4,5\text{-}B3OCn)_4pz]_x$ series included peaks at δ values of 9.34 [s (broad), 4H, pz] and 7.10 (s, 8H, H2/H6−C_6H_2−), in addition to the peaks corresponding to the aliphatic chains already mentioned for the dimers in all cases; those of the $[Rh_2(3,4\text{-}B2OCn)_4pz]_x$ series exhibited signals at δ values of 9.54 (s, 4H, pz), 7.54 (dd, 4H, H6−C_6H_3−, J = 8.4 Hz; J = 1.5 Hz), 7.44 (d, 4H, H2−C_6H_3−, J = 1.5 Hz), and 6.67 (d, 4H, H4−C_6H_3−, J = 8.4 Hz); and those of the $[Rh_2(3,5\text{-}B2OCn)_4pz]_x$ series exhibited peaks at δ values of 9.48 for n = 18 and 9.55 for n = 9 (s, 4H, pz), 7.01 (s, 8H, H2/H6−C_6H_3−), and 6.43 (s, 4H, H4−C_6H_3−). The fact that the four pyrazinic hydrogen atoms gave only one signal (shifted upfield by ca. 1 ppm with respect to free pyrazine) is strong evidence of its symmetrical coordination via both N atoms.

The pyrazine adducts were soluble in $CHCl_3$, and the complexes with two or three O-alkyl chains on the aromatic ring were also soluble in heptane, but all of them were insoluble in ethanol.

Strength of the pz−Rh Bond and Thermal Stability of the Pyrazine Adducts. From a synthetic point of view, the stoichiometric 1:1 polymeric adducts were easily obtained when the equatorial benzoate ligands bore longer aliphatic chains or when the two meta positions were substituted by aliphatic chains (3,5 and 3,4,5 substitution). This is probably because the O-axial coordination in solution (which gives rise to pseudopolymeric or oligomeric species) was not negligible with respect to the pyrazine axial coordination. The mentioned substitution patterns (3,5 and 3,4,5 substitution), as well as long chains, preclude the formation of these pseudo-polymeric species (by decreasing the equilibrium constant), thus favoring the formation of the pyrazine-polymerized structures.

Similar steric hindrance could be invoked to rationalize the pyrazine peak positions in the NMR spectra. In $[Rh_2(4\text{-}B1OC12)_4pz]_x$ compounds, this signal is at a lower field (10.24 ppm)[27] than in the $[Rh_2(3,4,5\text{-}B3OCn)_4pz]_x$ (9.34−9.48 ppm), $[Rh_2(3,4\text{-}B2OCn)_4pz]_x$ (9.54−9.55 ppm), and $[Rh_2(3,5\text{-}B2OCn)_4pz]_x$ (9.48−9.56 ppm) series. Compared to free pyrazine (8.63 ppm), these signals show a descreening due to coordination to the bimetallic center; however, the sensitivity of the descreening to the nature of the equatorial ligand shows that this effect is more pronounced in the case of the monosubstituted benzoate than in the others. This sequence probably reflects the proximity of pyrazine to the bimetallic center, showing that the axial ligand is more tightly bound to the 4-substituted systems than to the 3,4-disubstituted ones. Moreover, these latter species are more tightly bound than both the 3,5-disubstituted and 3,4,5-trisubstituted compounds. The aromatic ring showed a similar effect.

The strength of the Rh_2−pyrazine bond also depends on the substitution pattern on the equatorial benzoate ligands. This bond might be broken at high enough temperatures. To assess the thermal stability of the polymeric adducts (influenced by the Rh_2−pz bond strength, among others factors), we undertook a calorimetric study on one compound of each series. Pyrazine loss was detected at high temperatures; however, this process appeared to be quite slow, precluding the detection of the associated endothermic peaks in the DSC traces. For the same reason, as well as because the associated weight loss would be too small (<3%) for reliable measurements, TG experiments were discarded. Instead, several heating−cooling cycles were performed on each sample by DSC; the low-temperature limit was always room temperature, but the high-temperature limit was progressively raised from one cycle to another.

A comparison of the DSC traces thus obtained, including the appearance during the highest-temperature experiments of peaks characteristic of non-pyrazinic compounds, showed that compound **1b** started to decompose above 120 °C, whereas compounds **5b** and **8b** started to decompose at 150 °C. This slow process was accelerated when the samples were heated to temperatures 20−50 °C above those corresponding to the beginning of the reaction. These conclusions were extended to all of the members of each series; consequently, all thermal analyses aimed to characterize the phase sequences of these compounds were carried out

(35) (a) Wessemann, J. L.; Chisholm, M. H. *Inorg. Chem*. **1997**, *36*, 3258. (b) Wessemann, J. L.; Chisholm, M. H.; Christou, G.; Folting, K.; Huffman, J. C.; Samuels, J. A.; James, C. A.; Woodruff, W. H. *Inorg. Chem*. **1996**, *35*, 3643.

Table 2. Phase Transition Temperatures (in °C) and Enthalpies (in kJ/mol, in parentheses) for Each Compound Determined by DSC with Runs Conducted at 5 °C/min

compound	phase sequence[a]
1a	Cr—48 (275)—Col_H—156 (18)—I
2a	Cr—58 (195)[b,c]—Col_H—177 (19)—I
3a	Cr—55 (50)[b,c]—Col_H—189 (15)—I
4a	Col_R—43 (43)[d]—Col_R—228 (16)—I
5a	Cr—57 (190)[e]—Col_R—109 (13)—Col_H—175 (5)—I I—172 (−4)—Col_H—140 (−3)[c]—Col_H—54 (−181)[e]—Cr
6a	Cr—28 (58)—Col_R—120 (18)[c,e]—Col_H—213 (4)—I + Dec
7a	Cr_1—107 (1)—Cr_2—146 (19)—Col_H—250 (4)—I + Dec Col_H—143 (−15)—Col_R—115 (<−1)[c]—Cr
8a	Cr—45 (152)—Col_H—90 (23)—I
9a	Cr_1—107 (5)—Cr_2—119 (108)—I I—91 (−20)—Cr
1b	Cr—47 (375)[e,f]—Col_H
2b	Cr—36 (244)[b]—Col_H
3b	Cr—∼0 (120)[c]—Col_H
5b	Cr_1—39 (73)—Cr_2—82 (72)[e]—Cub Cub—90[g]—Col_R—34 (−131)—Cr_1
6b	Cr—92 (47)—Col_R[b]
8b	Cr_1—57 (10)[b]—Cr_2—68 (131)[e]—Col_N—126 (2)—I
9b	Cr_1—69 (5)[b]—Cr_2—110 (27)[e]—Col_N

[a] Abbreviations used: Col_H, columnar hexagonal phase *p6mm*; Col_R, columnar rectangular phase *p2gg*; Col_N, columnar nematic phase; Cub, cubic phase. Unless specified, the compounds showed quiet similar thermal behavior in the first cooling and subsequent heating/cooling cycles. [b] On cooling, the crystalization temperature is lower because of the strong supercooling of the mesophase. [c] Broad. [d] This transition does not appear upon cooling or additional heating−cooling cycles, even after long periods. [e] Double peak. [f] Double only in the first cycle. [g] No peak can be seen on DSC.

at temperatures below the point at which the loss of pyrazine occurs.

Phase Sequence and Mesomorphic Properties. The phase sequences, transition temperatures, and enthalpy changes were examined by polarized-light optical microscopy (POM), differential scanning calorimetry (DSC), and powder X-ray diffraction (XRD) studies. The results are summarized in Tables 2 (phase sequences, transition thermal parameters) and 3 (structural identification and structural parameters) and analyzed here for each series of compounds.

Rh_2(3,4,5-B3OC*n*)$_4$. Optical microscopic observation of compounds **1a**−**3a** showed a transition from a room-temperature crystalline phase into a mesophase exhibiting a texture with developing domains (Figure 3a for compound **2a**). For the compound with $n = 10$, the transition extended over a wide range of temperature. This behavior was reversible whatever the scanning rate, both in POM and DSC experiments. The 2-D hexagonal symmetry of this mesophase (Col_H) was confirmed by XRD studies: the diffraction patterns were characterized by a series of peaks in the small-angle region corresponding to reciprocal spacings in the ratio $1:\sqrt{3}:\sqrt{4}:\sqrt{7}$ and to the indexing $hk = 10$, 11, 20, and 21 and also by a wide halo centered at ca. 4.5 Å characteristic of liquidlike order. No evidence of a long-range intracolumnar order could be found. These observations are consistent with the mesomorphic behavior already found[27] for compound **3a**, even if there are minor differences in the thermodynamic parameters. The lower homologue studied, compound **4a**, showed a markedly different optical texture (Figure 3b) that changed slightly with temperature. The XRD patterns of this mesophase were characterized by two intense reflections in the small-angle region (the one at the smallest angle being the more intense of the two reflections), accompanied by a series of weaker peaks in the middle-angle region and the typical halo at 4.5 Å in the wide-angle region. These patterns correspond to a columnar rectangular (Col_R) mesophase. The two intense small-angle reflections were assigned as $hk =$ 11 and 20, allowing for the complete indexing of the other peaks. The presence of the 34 reflection ($h + k \neq 2n$) allowed us to identify the two-dimensional space group of the rectangular columnar phase as *p2gg*. The indexing given in Table 3 is that obtained for the Col_R phase at 100 °C and was reproducible on subsequent heating−cooling cycles. It is interesting to note that another Col_R mesophase was detected at lower temperature but only in the first heating, and it was not observed again (even after annealing the sample for several hours at ambient temperature). The same *p2gg* 2D-space group was determined by XRD with only small variations of the intercolumnar distance (and therefore of the cell dimensions *a* and *b* and the cross-columnar section).

Rh_2(3,4-B2OC*n*)$_4$. As observed by POM, on heating, compounds **5a**−**7a** exhibited two main changes before clearing: on melting, the formation of a dark texture was observed, from which a brighter birefringent texture slowly developed (Figure 3c); approximately 40 °C higher, it transformed into another birefringent texture. This behavior is in agreement with the two peaks detected in the DSC traces and with the XRD experiments. The high-temperature phase was identified in the three cases as a Col_H phase. Below this mesophase, a stable enantiotropic Col_R phase was seen for **6a**, whereas **7a** exhibited a monotropic Col_R phase. For **5a**, a Col_R phase was detected in the first heating only, giving place to a second hexagonal phase on cooling and subsequent thermal cycles. This phase sequence (Col_R−Col_H) was observed for the $n = 10$ homologue.[27]

Rh_2(3,5-B2OC*n*)$_4$. Complex **8a** exhibited a transition from a crystalline phase into a Col_H mesophase, whereas complex **9a** is not mesomorphic.

For the three series just analyzed, it has to be highlighted that no peak that could be assigned to an intracolumnar distance was seen in the diffractograms. Thus, the LC phases of these compounds can be seen as consisting of a long-range-ordered two-dimensional arrangements of columns formed by piled cores but without any long-range order between the position of the cores within the columns. The absence of any long-range intracolumnar order might be due to the steric hindrance of the bulky alkoxybenzoic ligands, which prevent the dimers from approaching one another, thus precluding strong intermolecular interactions (coordination bonds, $\pi-\pi$ interactions). The molecular organization within the mesophases is analyzed in more details in the Discussion section.

[Rh_2(3,4,5-B3OC*n*)$_4$pz]$_x$. In contrast to all previously reported pyrazine-bridged bimetallic carboxylates,[22b,f,g,27,28] compounds **1b**−**3b** each exhibited a thermotropic mesophase. The transition from the crystalline to the LC phase was reversibly detected for **1b** by POM (see the texture on Figure 3d that show defects similar to broken fans), DSC, and XRD and found to take place below room temperature for compounds **2b**

Table 3. Detailed Indexing at a Given Temperature of All LC Phases[a] of Each Compound

	phase (T/°C)	d_{obs}[b]	I[c]	hk[d]	d_{calc}[e]	cell parameters[f]
1a	Col_H	29.5	VS	10	29.5	$D = 34.1$
	$p6mm$	16.9	M	11	17.1	$S = 1007.5$
	(110)	14.6	M	20	14.8	
		11.1	W	21	11.2	
2a	Col_H	26.8	VS	10	26.8	$D = 30.9$
	$p6mm$	15.5	M	11	15.5	$S = 828.7$
	(110)	13.4	M	20	13.4	
		10.1	W	21	10.1	
3a	Col_H	23.4	VS	10	23.4	$D = 27.1$
	$p6mm$	13.6	M	11	13.5	$S = 634.2$
	(110)	11.7	M	20	11.7	
		8.9	W	21	8.9	
4a	Col_R	21.7	VS	11	21.7	$a = 38.1$
	$p2gg$	19.0	S	20	19.0	$b = 26.4$
	(100)	13.2	M	02	13.2	$S = 1004.8$
		11.5	W	31	11.4	
		10.8	VW	22	10.8	
		9.6	VW	40	9.5	
		8.6	VW	13	8.6	
		7.3	VW	33	7.2	
		6.3	VW	24	6.2	
		5.8	VW	34	5.9	
		5.4	VW	44	5.4	
5a	Col_R	32.4	VS	11	32.4	$a = 61.2$
	$p2gg$	30.6	S	20	30.6	$b = 38.2$
	(70)	19.0	M	02	19.1	$S = 2336.6$
		17.7	M	31	18.0	
		16.2	W	22	16.2	
		15.3	W	40	15.3	
		11.7	VW	23	11.8	
5a	Col_H	32.3	VS	10	32.3	$D = 37.3$
	$p6mm$	18.6	M	11	18.6	$S = 1201.3$
	(110)	16.1	M	20	16.2	
		12.2	W	21	12.2	
6a	Col_R	29.3	VS	11	29.3	$a = 54.1$
	$p2gg$	27.1	S	20	27.1	$b = 34.9$
	(70)	17.3	M	02	17.4	$S = 1887.2$
		16.0	W	31	16.0	
		14.6	W	22	14.7	
		13.8	W	40	13.5	
		11.3	VW	14	11.4	
6a	Col_H	29.1	VS	10	29.1	$D = 33.7$
	$p6mm$	16.9	M	11	16.8	$S = 980.3$
	(110)	14.5	M	20	14.6	
		11.1	W	21	11.0	
7a	Col_H	23.9	VS	10	23.9	$D = 27.5$
	$p6mm$	13.9	M	11	13.8	$S = 657.0$
	(160)	12.0	M	20	12.0	
		9.1	W	21	9.1	
7a	Col_R	25.4	VS	11	25.4	$a = 45.7$
	$p2gg$	22.9	S	20	22.9	$b = 30.5$
	(130[g])	15.2	W	02	15.3	$S = 1393.7$
		13.5	W	31	13.6	
		11.3	W	40	11.4	
8a	Col_H	31.2	VS	10	31.2	$D = 36.1$
	$p6mm$	18.1	M	11	18.0	$S = 1125.3$
	(70)	15.7	M	20	15.6	
		11.9	W	21	11.8	
		10.4	W	30	10.4	
		8.6	W	22	8.7	
		5.8	M	33	5.9	
				42	6.0	
1b	Col_H	26.2	VS	10	26.2	$D = 30.3$
	$p6mm$	15.1	M	11	15.2	$S = 794.6$
	(90)	13.1	M	20	13.1	
		10.0	W	21	9.9	
		8.9	W	Stack		
2b	Col_H	23.9	VS	10	24.0	$D = 27.7$
	$p6mm$	13.8	S	11	13.8	$S = 662.2$
	(90)	12.0	M	20	12.0	
		8.9	W	Stack		
3b	Col_H	21.5	VS	10	21.5	$D = 24.8$
	$p6mm$	12.4	M	11	12.4	$S = 532.7$
	(90)	10.8	M	20	10.7	
		8.0	W	21	8.1	
5b	Cub	29.4	VS	100	29.4	$a = 29.4$
	(110)	20.8	M	110	20.8	
		17.0	W	111	17.0	
		14.6	VW	200	14.7	
5b	Col_R	31.2	VS	11	31.2	$a = 53.5$
	$p2gg$	26.7	S	20	26.7	$b = 38.3$
	(60[g])	18.0	VW	12	18.0	$S = 2049.0$
		15.6	M	22	15.6	
6b	Col_R	28.5	VS	11	28.5	$a = 52.2$
	$p2gg$	26.1	S	20	26.1	$b = 34.0$
	(80[g])	16.5	W	12	16.2	$S = 1775.7$
		14.3	W	22	14.3	
		12.5	VW	41	12.2	
		10.7	W	23	10.4	
		7.7	W	34	7.7	
8b	Col_N	24.4	VS	10		
	(110)	8.7	M	Stack		
9b	Col_N	18.4	VS	10		
	(120)	8.8	M	Stack		

[a] Except where specified, the phase are the one obtained on heating. [b] d_{obs} = observed spacing (Å). [c] I = intensity of the diffraction signal. [d] hk = indexing of the lattice. [e] d_{calc} = calculated spacing (Å). [f] D = intercolumnar distance for the columnar hexagonal phases (Å); S = lattice area (Å^2); a, b = lattice parameters for the columnar rectangular phases (Å). [g] Not the phase obtained on heating.

and **3b**. Thermodynamic and structural parameters are reported in Tables 2 and 3. This mesophase was identified as a hexagonal columnar phase with long-range intracolumnar order: the peaks in the small-angle region correspond to reciprocal spacings in the ratio 1:√3:√4:√7, the wide halo centered at ca. 4.5 Å is characteristic of the liquidlike order, and the broad scattering detected in most of the diffraction patterns at 8.7−8.9 Å is associated with the intracolumnar periodicity. The use of the Scherrer expression,[36] which correlates the position of the Bragg peak and its width at half-height with the domain size, allowed for a rough estimation of the correlation length, which was evaluated to be 75 Å, corresponding to the stacking of 8−9 repeat units.

[Rh$_2$(3,4-B2OCn)$_4$pz]$_x$. Microscopic observation was not conclusive in the characterization of the mesophases exhibited by the two homologues **5b** (at high temperatures, it has a viscous isotropic phase that becomes birefringent on cooling) and **6b** (its fluid high-temperature phase has a birefringent texture). For the n = 18 homologue (**5b**), XRD studies allowed the higher-temperature isotropic phase to be identified as cubic (Cub): the small-angle region contained a series of peaks corresponding to reciprocal spacings in the ratios 1:√2:√3:√4. This mesophase transforms into a Col_R phase on cooling (monotropic phase) without showing any detectable enthalpy change. The intracolumnar stacking was found to be slightly shorter than in the preceding series: 7.5−7.6 Å. The correlation length was estimated to be 17 repeat units per column (130 Å). At this point, it is not possible to determine the 3-D space

(36) Weller, M. *Inorganic Materials Chemistry*; Oxford University Press: New York, 1996.

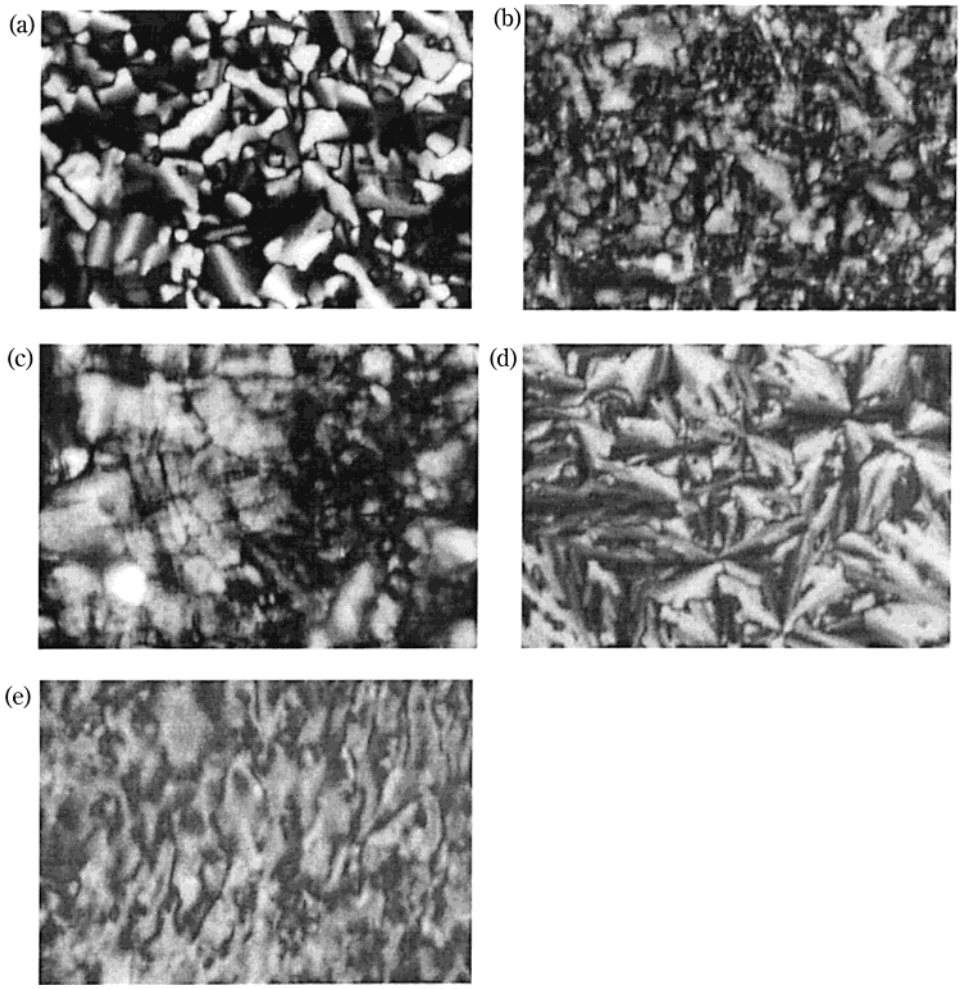

Figure 3. Selected optical textures characteristic of the mesophases detected for various studied compounds: (a) **2a** at 150 °C, (b) **4a** at 105 °C, (c) **6a** at 92 °C, (d) **1b** at 130 °C, (e) **8b** at 114 °C.

group or to discriminate between a micellar or bicontinuous cubic structure. For the $n = 14$ homologue (**6b**), the high-temperature phase was identified as a Col_R phase.

$[Rh_2$(3,5-B2OC*n*)$_4$pz$]_x$. The crystalline phase of both complexes **8b** and **9b** is followed at higher temperatures by a mesophase that showed XRD patterns containing three broad peaks: a first one at 24 Å ($n = 18$) or 18 Å ($n = 9$), a second one at ca. 8.7 Å, and a third broad one at ca. 4.5 Å. The first and third peaks are typical of nematic (N) or liquid phases. The birefringent texture (see Figure 3e) confirmed the LC character of this phase, which was thus assigned as a Col_N phase: the rodlike units are columns of $[Rh_2(3,5\text{-}B2OCn)_4pz]_x$ oligomers, with an internal periodicity of 8.7 Å along the columnar axis. The correlation length within each column was estimated to be 80 Å, corresponding approximately to 9 Rh_2-pz units.

Most of the compounds (pyrazine-bridged and non-pyrazine-bridged) retain their 2-D columnar hexagonal or rectangular arrangement when they crystallize. The kinetics of crystallization of some of the compounds under study, particularly the ones with short O-alkyl chains, are quite slow.

Discussion

The procedure followed to synthesize the polymeric compounds was found to be useful in overcoming the complex equilibria involving different pyrazine adduct species in solution; indeed, only the polymeric 1:1 species were obtained. The XRD experiments allowed for a complete characterization of all of the obtained mesophases. The nature of the LC phases of the compounds was determined by the pattern of substitution on the aromatic ring as well as the length of the O-alkyl chains. The influence of both factors (position and length of chains) on the mesomorphic properties of polycatenar calamitic metallomesogens has been analyzed in detail in terms of the curvature of the paraffinic/aromatic interface.[37]

To gain deeper insight into the structural features of the mesophases exhibited by these compounds, we tried to establish suitable models for their supramolecular organization. Because, as far as we know, there are no reports on the crystalline structure of dirhodium carboxylates either axially bridged to form polymers or bearing substituted benzoates, these models are based on the crystalline structures of the related rhodium carboxylate bis-adducts $[Rh_2(O_2CPh)_4(C_5H_5N)_2]$[38] and $[Rh_2(O_2CPh)_4(DMSO)_2]$.[39]

The first structural parameter to be considered is the intracolumnar periodicity, *h*. Following the usual

(37) Donnio, B.; Bruce, D. W. *New J. Chem.* **1999**, 275.
(38) Mehmet, N.; Tocher, D. *Inorg. Chim. Acta* **1991**, *188*, 71.
(39) Simmons, C.; Clearfield, A.; Sun, Y. *Inorg. Chim. Acta* **1986**, *L3*, 121.

approach in the structural analysis of columnar mesophases,[16,17,40] the volume of one columnar repeat unit, centered on one node of the hexagonal array, with transverse section area S and height h, can be expressed as

$$V = Sh = pV_o \quad (1)$$

where V_o is the volume of one dimer and p is the number of dimers within the columnar slice (for Col_H mesophases, the columnar cross section agrees with the unit cell area; for Col_R ones, p should include the presence of two columns per unit cell if the unit cell area is used for S). With the hypothesis of additivity of partial volumes, the volume V_o can be written as

$$V_o = V_{pc} + 4m(nV_{CH_2} + \Delta V_{CH_3}) \quad (2)$$

where m is the number of alkoxy chains on each aromatic ring, V_{pc} is the molecular volume of the polar core, and $(nV_{CH_2} + \Delta V_{CH_3})$ is the volume of one aliphatic chain of n carbon atoms. Replacing the expression for V_o from eq 2 into eq 1, the cross-sectional area of a column is obtained as

$$S = (p/h)(V_{pc} + 4m\Delta V_{CH_3}) + (p/h)(4mV_{CH_2})n \quad (3)$$

The first term is constant (for each series at a given temperature) as a function of n, whereas the second increases linearly with n. The ratio p/h can be calculated from the slope of S as a function of n obtained by linear regression. The volume of one methylene group, $V_{CH_2}(T)$, for aliphatic chains in a disordered conformation was taken from the litterature[41] as $V_{CH_2}(T) = 25.922 + (2.076 \times 10^{-2})T$ (Å^3), where the temperature T is in °C.

Estimations were performed for the mesophases of the three compounds for which enough information was available, namely, the Col_H phase of Rh_2(3,4,5-B3OCn)$_4$ (n = 10, 14, and 18), the Col_H phase of Rh_2(3,4,5-B3OCn)$_4$pz (n = 10, 14, and 18), and both the Col_H and Col_R mesophases of Rh_2(3,4-B2OCn)$_4$ (n = 9, 14, and 18). These calculations were made for each series of compounds at different temperatures, on heating, and on cooling; a value of h/p was calculated for each of them. Figure 4 shows the variation of S as a function of n at one selected temperature in each series. To confirm these calculated h values, the mean molecular volume (V_o) derived from the XRD data (Sh/p) was compared with estimated molecular volumes (V_e; see Appendix A for these calculations). The validity of the calculated V_e values was also checked by comparing room-temperature V_e values with the molecular volume resulting from experimental density measurements, V_d. Some representative results are given in Appendix A.

Series Rh_2(3,4,5-B3OCn)$_4$. As previously mentioned, the columnar mesophase of these compounds did not present any peak that could be assigned to the intracolumnar repeat distance, so the stacking arrangement is probably disordered. The deduced mean value h = 7.2 ± 0.4 Å (assuming p = 1) is not comparable with direct experimental measurements; however, the feasibilty of some possible superstructures can be analyzed.

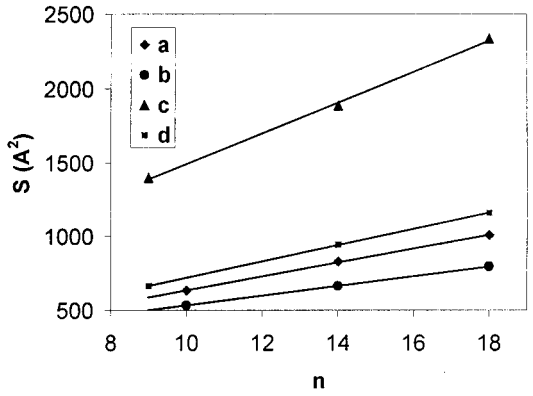

Figure 4. Unit cell area as a function of the number of carbon atoms in each alkyl chain for the following series and mesophases: (a) Col_H Rh_2(3,4,5-B3OCn)$_4$ (T = 110 °C), (b) Col_H [Rh_2(3,4,5-B3OCn)$_4$pz]$_x$ (T = 90 °C), (c) Col_R Rh_2(3,4-B2OCn)$_4$ (T = 70 °C for n = 14 and 18 on heating and T = 120 °C for n = 9 on cooling), (d) Col_H Rh_2(3,4-B2OCn)$_4$ (T = 150 °C). The solid lines correspond to linear regressions.

A pseudopolymeric structure based on Rh···O (neighbor carboxylate) axial coordination, similar to that found in the aliphatic analogues,[22e,24] would give rise to a repeat distance of 5.2 Å (Figure 5a), too small with respect to the 7.2 Å calculated value, and has to be ruled out. A second possibility is to consider columns formed by piled dimers having both axial positions free of coordinated atoms (i.e., the rhodium atoms have a square-pyramidal geometry, Figure 5b). Alternatively, it is possible to assume that the axial positions are occupied by oxygen atoms of the ether groups of the neighboring dimers, instead of the oxygen atoms belonging to the carboxylate moieties (Figure 5c). With the second assumption, there is neither a maximum possible distance nor a more probable distance other than that resulting from the contact van der Waals radii, which, in turn, depends on the torsion angle aromatic plane/Rh_2 bond. In that case, the compounds would probably tend to give nematic discotic phases instead of columnar phases. With the third assumption, the longest possible distance between two rhodium atoms of adjacent dimers would be near 8.5 Å if both Rh−Rh bonds and the aromatic core between them were coplanar; if they were not in the same plane, this distance would be shorter. As no structure of rhodium benzoates without axial ligands has been published, it is not possible to make a decision by means of comparison with known structures. Indeed, to differentiate between these two possibilities, some kind of local probe, such as EXAFS, would be useful. Alternatively, the synthesis and characterization of the alkyl analogues (without ether functional groups on the aromatic core) could be informative.

Series [Rh_2(3,4,5-B3OCn)$_4$pz]$_x$. The measured 8.9−9 Å stacking distance is slightly shorter than the value expected for the repeat unit of the polymeric chain (Rh_2−pz) in a completely extended conformation, which was evaluated by the addition of crystallographic interatomic distances as 9.6−9.7 Å (Figure 5d). This probably suggests a slightly bent conformation (Rh−Rh−N and Rh−N−N angles smaller than 180°), as has already been found in some Ru_2−phenazine compounds.[42] On the other hand, the value obtained for h/p

(40) Levelut, A. M. *J. Chim. Phys.* **1983**, *80*, 149.
(41) Guillon, D.; Skoulios, A.; Benattar, J. J. *J. Phys.* **1986**, *47*, 133.
(42) Cotton, F. A.; Kim, Y.; Ren, T. *Inorg. Chem.* **1992**, *31*, 2723.

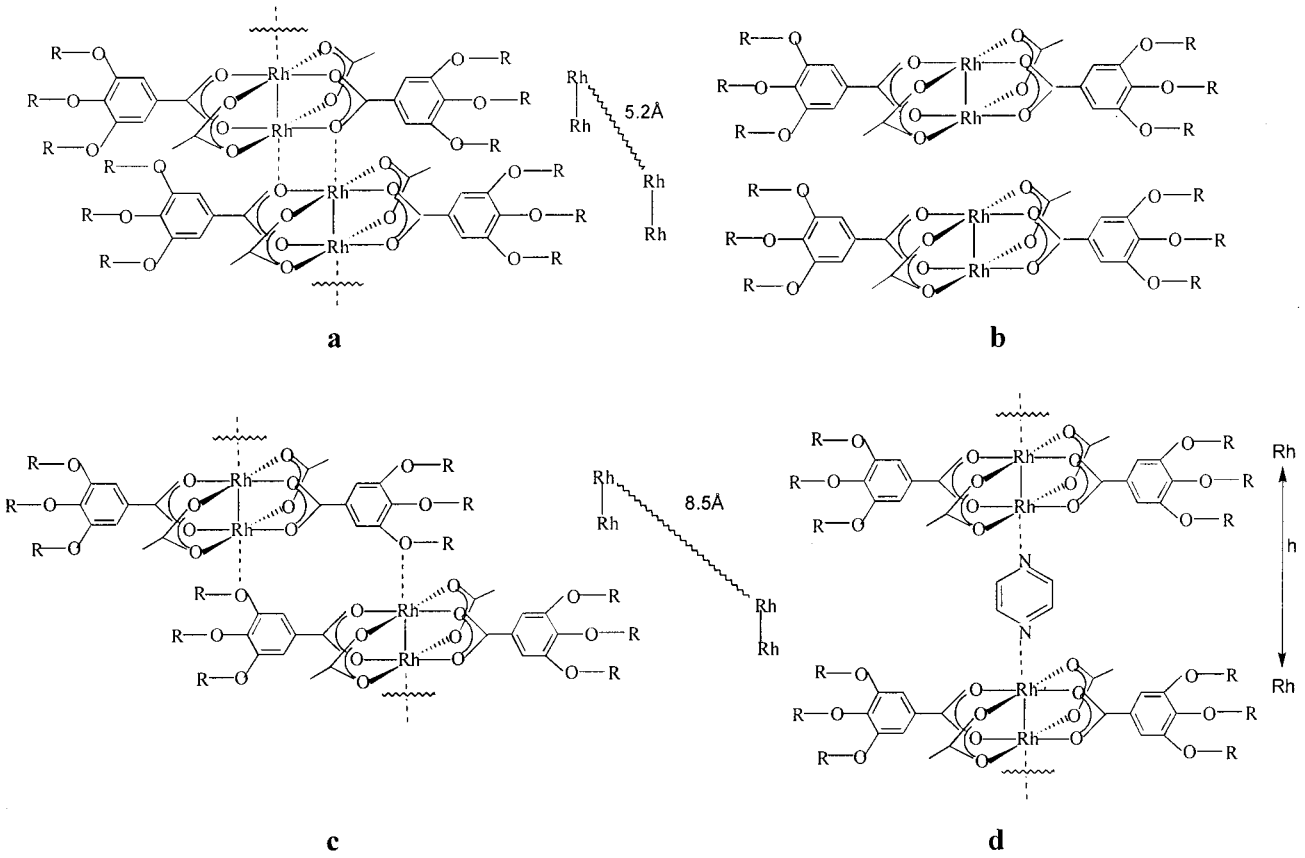

Figure 5. Scheme of proposed molecular models for Rh_2(3,4,5-B3OC*n*)$_4$ series with and without pyrazine. (a−c) Col$_H$ Rh_2(3,4,5-B3OC*n*)$_4$, (d) Col$_H$ [Rh_2(3,4,5-B3OC*n*)$_4$pz]$_x$.

by linear regression of the plot of *S* vs *n* is nearly 10−10.2 Å. This small difference might be due to the incomplete fulfillment of the hypothesis of the model used for calculation. One possible explanation is that, in the regions near the ···Rh_2−pz··· central chain, the space is not completely filled by the aliphatic chains, whose conformational disorder gives a liquidlike character beyond the aromatic parts.

Series Rh_2(3,4-B2OC*n*)$_4$ Col$_R$ Phase. As stated above, this mesophase has short-range stacking order because there is no X-ray signal that could be assigned to the intracolumnar repeat distance. From Figure 4, *h*/*p* was calculated as 1.95 Å. Because of the rectangular symmetry of the mesophase, *p* has to be an even number. The possibility of $p = 2$ can be elimated as it implies that $h = 3.90$ Å, smaller than the minimum calculated distance between rhodium atoms of two adjacent dimers (5.2 Å). It thus seems reasonable to suggest that $p = 4$; in this case, the intracolumnar repeat distance is close to 7.8 Å (Figure 6), a distance that can be interpreted similarly to the one obtained for the Rh_2(3,4,5-B3OC*n*)$_4$ series. This assumption ($p = 4$) means that each of the two lattice points of the unit cell of the bidimensional columnar centered rectangular mesophase is formed by two disordered chains of dimers. Such a situation (columns made up by more than one molecular strands) has already been suggested for systems having a low density of alkyl chains, associated with void space to be filled.[17] Indeed, this is also the case in the 3,4-disubstituted benzoates, where the presence of only two alkoxy chains per aromatic ring with some separation between neighbor dimers provides enough room to locate (or be interpenetrated by) the aliphatic chains of the dimers that constitute the second chain of this particular lattice point of the net. The comparison of the unit cell surfaces with those of the Rh_2(3,4,5-B3OC*n*)$_4$ compounds supports this hypothesis (see next section).

Series Rh_2(3,4-B2OC*n*)$_4$ Col$_H$ Phase. The same facts as in the previous case suggest that these compounds show a columnar hexagonal mesophase with no order of stacking. The value of *h*/*p* obtained from the plot is 4.50 ± 0.55 Å, with a particularly high variation with temperature.

Similarly to the case of the columnar rectangular mesophase, it can be concluded that the number of dimers within that columnar section (*p*) is two; then, the repeat distance would be 7.9 at 110 °C and 10.1 Å at 170 °C. This fact can also be explained in the same terms as in the previous case (Figure 6b). The comparison of the unit cell surfaces of these compounds (890 Å^2 for $n = 14$ at 180 °C) with those corresponding to the trisubstituted analogues (846 Å^2 for $n = 14$ at 170 °C) is an additional indication of the presence of columns made up of "double chains" of dimers.

Conclusions

The application of a strategy designed to fill intrinsically the intermolecular space in "ionic" polymeric diruthenium carboxylates was successful also in the present case ("neutral" coordination polymers). Indeed, the use of bulky equatorial carboxylates allowed the mesomorphic character of the pyrazine-polymerized dirhodium carboxylates to be preserved. The structural

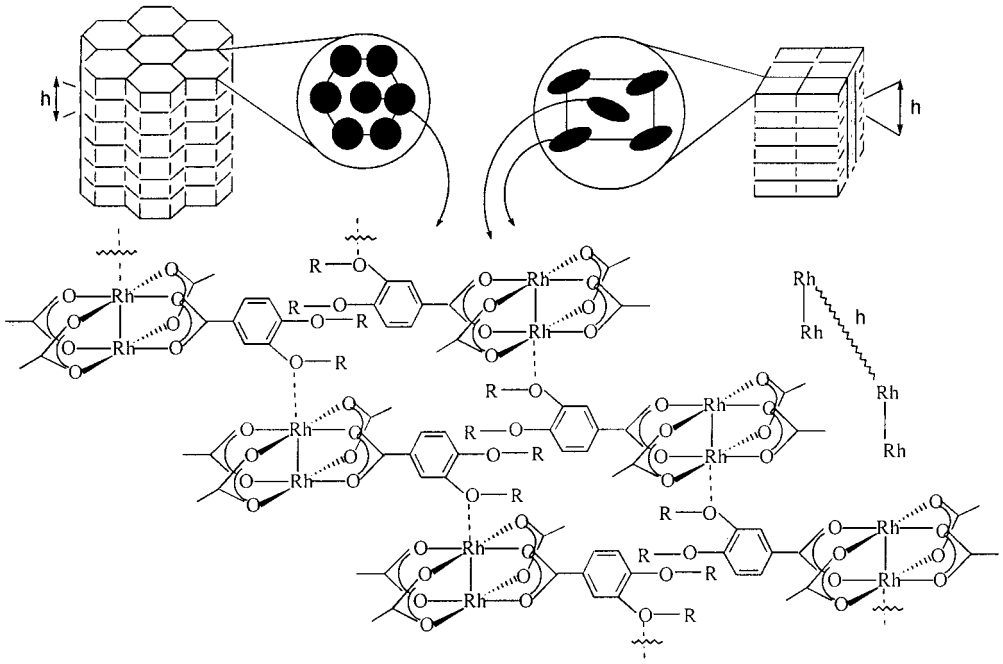

Figure 6. Scheme of proposed molecular models for $Rh_2(3,4\text{-}B2OC\textit{n})_4$ series in the Col_R and Col_H phases.

characterization of the mesophases exhibited by the three different polymeric series showed the occurrence of columnar phases with different structures, including nematic, hexagonal, and rectangular ones. In addition, the mesomorphic behavior of the nonadduct precursors was also assessed. In both cases, supramolecular models were proposed to explain the main structural features of the observed mesophases. The substitution pattern on the aromatic ring, the aliphatic chain length, and the presence of axial pyrazine play an essential role in the definition of the precise structure (hexagonal, rectangular, cubic, or nematic; ordered or disordered) of the mesophase and can be used to tune its nature.

These results show that it is possible to obtain polymeric columnar metallomesogens in which the electron-rich metallic centers are connected by communicating ligands, giving rise to structures that eventually can act as molecular wires. To make improvements in this direction, different aspects have to be optimized: the possibility of obtaining long-range polymeric structures along the columnar axis and macroscopically oriented samples, the increase in the interdimeric interactions, and the use of metals having a more suitable electronic structure. All of these options are currently under study in our laboratories; in particular, the use of divalent ruthenium carboxylates $[Ru_2(B\textit{m}OC\textit{n})_4pz]_x$ seems to be a promising approach. This last series has the disadvantage of being air-unstable when no axial ligands are present, but presenting a paramagnetic $S = 1$ ground state (eventually leading to magnetically oriented mesophases) and a partly filled HOMO orbital, a good strating point for looking for electronic conductivity.

Acknowledgment. We thank Dr. Benoît Heinrich (GMO−IPCMS) for his kind assistance in the X-ray determinations and Zulema Chaia (Inquimae) for her interesting suggestions. Grants from the University of Buenos Aires (AX27), Conicet (PEI 221/97), ANPCyT (546), and Setcip-Ecos (International Cooperation A97E08), as well as a fellowship from Conicet to M.R. supported this work. F.D.C. is a member of the research staff of Conicet.

Appendix

The molecular volumes of the analyzed compounds were calculated by adding the contributions of the different molecular parts, as follows:

For the non-pyrazine-bridged molecules

$$V_{\text{molecule}} = V[Rh_2(\text{benzoate})_4] + V[OCH_3]4m + V[CH_2](n-1)4m$$

For the polymers

$$V_{\text{repeat unit}} = V[Rh_2(\text{benzoate})_4] + V[OCH_3]4m + V[CH_2](n-1)4m + V[\text{pz}]$$

The value used for $V[Rh_2(\text{benzoate})_4]$ (631.5 Å^3) was estimated as $V[Rh_2(\text{benzoate})_4(Py)_2] - 2V[Py]$; the former volume was taken from the literature,[38] and the molecular volume of pyridine was calculated from its density value. The volume of the OCH_3 groups was estimated as 37 Å^3 as $V[Ru_2(4\text{-}B1OC1)_4Cl]1.25H_2O - V[Ru_2(\text{benzoate})_4Cl] - 0.25V[H_2O]$,[43] and the volume of pz (129 Å^3) was calculated in the same way as the volume of pyridine. For the CH_2 group, the same values as before were used.

The agreement of the values obtained by these methods can be seen in the following selected values: for **1a**, V_o(110 °C) = 7200 Å^3, V_e(110 °C) = 6900 Å^3; for **1b**, V_o(90 °C) = 7050 Å^3, V_e(90 °C) = 6950 Å^3; for **3a**, V_o(110 °C) = 4500 Å^3, V_e(110 °C) = 4200 Å^3, V_o(25 °C) = 3980 Å^3, V_d(25 °C) = 4200 Å^3; and for **8a**, V_e(25 °C) = 4550 Å^3, V_d(25 °C) = 4550 Å^3.

CM0109995

(43) (a) Abe, M.; Sasaki, Y.; Yamaguchi, T.; Ito, T. *Bull. Chem. Soc. Jpn*, **1992**, *65*, 1585. (b) Das, B.; Chakravarty, A. *Polyhedron* **1991**, *10*, 491.